Strength, microstructure, and life cycle assessment of silicomanganese fume, silica fume, and Portland cement composites designed using Taguchi method

Muhammad Nasir: Department of Civil and Construction Engineering, College of Engineering, Imam Abdulrahman Bin Faisal University, Dammam 31451, Saudi Arabia; mnmuhammad@iau.edu.sa; (*first author*; *corresponding author*).

Adeyemi Adesina: Department of Civil and Environmental Engineering, University of Windsor, Windsor, Ontario, Canada; adesina1@uwindsor.ca; (*second author*).

Ashraf A. Bahraq: Interdisciplinary Research Center for Construction and Building Materials, King Fahd University of Petroleum & Minerals, Dhahran 31261, Saudi Arabia; ashraf.bahraq@kfupm.edu.sa; (third author).

Muhammad Arif Aziz: Department of Civil and Construction Engineering, College of Engineering, Imam Abdulrahman Bin Faisal University, Dammam 31451, Saudi Arabia; maaahmed@iau.edu.sa; (fourth author).

Aziz Hasan Mahmood: School of Civil and Environmental Engineering, University of Technology Sydney (UTS), Ultimo NSW 2007, Australia; aziz.mahmood@uts.edu.au; (fifth author; corresponding author).

Mohammed Ibrahim: Applied Research Center for Metrology, Standards and Testing, Research Institute, King Fahd University of Petroleum and Minerals, Dhahran 31261, Saudi Arabia; ibrahim@kfupm.edu.sa; (sixth author).

Moruf Olalekan Yusuf: Department of Civil Engineering, University of Hafr Al-Batin, Hafr Al-Batin 31991, Saudi Arabia; moruf@uhb.edu.sa; (seventh author).

Abstract

The incorporation of supplementary cementitious materials (SCMs) into cementitious materials canbe used to offset the overall carbon footprint of cement in addition to improving perfofmance and promoting circular economy. Synthesized silicomanganese fume (SiMnF), silica fume (SF), and ordinary Portland cement (OPC) based binary and ternary cementitious mortar specimens were designed and optimized using the Taguchi method. Four factors with three levels each were investigated –SiMnF content of 0-40% and SF content of 0-10% (by mass) of the total cementitious, sand-to-binder of 1.5-2.5, and water-to-binder ratio of 0.35-0.45. Based on the orthogonal array proposed by the Taguchi method, nine mortar mixes were batched and their flow after mixing and compressive strength at 3, 7, and 28 days of casting were measured. The strength data were statistically analyzed using ANOVA to investigate the effects of the chosen experimental variables. It was observed that the strength is considerably reduced from the addition of SiMnF, but the reduction is marginal from increasing the sand-to-binder ratio. The addition of 5% SF increased the strength. A restricted analysis indicated that specimens prepared with 20% SiMnF, or 20% SiMnF and 5% SF can yield mortar strengths of up to 30.5 MPa and 48.8 MPa, respectively. Microstructural investigations revealed that the mixes with SiMnF have detectable pores at x1000 magnification, however, the addition of 5% SF densifies the matrix with no visible pore at the same magnification. This corroborates the strength data. The life-cycle assessment (LCA) indicates that the utilization of SiMnF in the mortar mixtures can reduce CO_2 emissions by up to 25% at a reasonably acceptable compressive strength.

Keywords: Silicomanganese fume; Silica fume; Taguchi method; Compressive strength; Microstructure; Life cycle assessment.

1. Introduction

The cement industry, being one of the most carbon-intensive manufacturing sectors, is a well-recognized CO_2 emission source (Santos et al. 2021). The production of Portland cement is associated with over 5-8% of the world's human-induced CO_2 emissions (Gao, Shen et al. 2016) and is predicted to rise as the demand for cement in concrete manufacture for infrastructural development is continually going up. With a growing interest in sustainable practices, the high emission potential of the cement and construction industry has been recognized and several innovative engineering solutions have been realized to reduce and manage its carbon footprint. Backed by decades of research, the use of supplementary cementitious materials (SCMs) has been identified as a promising avenue in reducing the carbon footprint of cement and by extension, of concrete (Anurag et al. 2021; Arrigoni et al. 2020). As SCMs are predominantly industrial byproducts and wastes, their utilization in concrete does not just offset the overall carbon footprint of cement, it also allows the use of end-of-life wastes within a circular economy. The use of SCMs as cement replacement has also been recognized to offer concrete durability which essentially extends the design life of structures; concrete assets need not be replaced as often as with a relatively low-durable product. This also offers a sustainable approach as the demand for concrete, at least in replacing like-for-like concrete, is kept reasonably limited.

Backed by research and trial data, the use of SCMs and other mineral additions to cement is often regulated, for instance, Australian Standard AS 3972 general purpose and blended cements allows the use of up to 20% mineral additions. This extends to State specifications such as the Transport for New South Wales (TfNSW) QA Specification 3211 outlines provisions for the use of fly ash, ground granulated iron blast-furnace slag (GGBFS), amorphous silica, and powdered glass as SCMs. There are specific standards to regulate the quality of SCMs too, for instance, AS 3582 supplementary cementitious materials for use with Portland and blended cement has three parts AS 3582.1, AS 3582.2, and AS 3582.3 covering specifications for fly ash, GGBFS, and amorphous silica. This demonstrates the reliability of SCMs and as such, the demand for SCMs is on the rise. A recent report by the American Coal Ash Association (ACAA) (American Coal Ash Association (ACAA) 2017) has estimated that fly ash production (more appropriately, generation) has dropped by about 40% while the demand has almost doubled between 2000 and 2017. This is a combined effect of the realization of the benefits of fly ash while the energy sector is shifting towards alternative green sources of electricity moving away from coal-powered power plants, the suppliers of fly ash. This creates an avenue to investigate alternative SCM sources in understanding their contribution to concrete strength, microstructure, and impact on the environment as such alternatives are likely to compensate for the higher demand for SCMs in the near future.

One promising alternative to traditional SCMs is silico-manganese fume (SiMnF), a by-product of the ferroalloy industry, which is usually stored at the plant before being disposed of at landfills which essentially makes it a waste product. Owing to its chemical composition of being rich in amorphous silica, magnesium, and potassium, SiMnF possesses the potential to be incorporated into concrete manufacture as an SCM. Studies on SiMnF as an SCM are very limited although it has been successfully utilized as a precursor in alkali-activated composites (Nasir et al. 2020, 2021c). One study on the utilization of SiMnF in producing self-compacting concrete was reported by Gawah et al. (Gawah et al. 2022). The study reports the use of SiMnF in effectively reducing CO_2 emissions, with a reduction in the range of 10–68%, depending on the SiMnF content (10–70%). However, this study reported only an elementary estimation of the CO_2 emissions by varying the SiMnF content which leaves opportunities for a detailed life cycle assessment (LCA) study on SiMnF binary and ternary (through the incorporation of silica fume) blended binders. The LCA is gaining attention at a commercial level while major suppliers of cement and concrete are through regulations, specified to undertake environmental product declarations that quantify emissions of a product on its life cycle to enable comparisons between alternatives.

To that extent, the primary aim of the current study is designed around investigating the synergistic influence of silicomanganese fume and silica fume as SCMs on cement mortar composites including other design variables such as the sand-to-binder ratio and water-to-cementitious ratio. The Taguchi method has been employed for the design and optimization of the mortar mixes. The corresponding performance of the composites was evaluated in terms of the fresh, mechanical, and microstructural properties. A comprehensive LCA was also carried out to assess the various environmental impacts of the mixes. This study will promote the valorization of the SiMnF industrial waste, minimize the associated environmental risks and cost of landfilling, and contribute towards achieving the Sustainable Development Goals (SDGs) and net-zero targets.

2. Experimental program

2.1. Taguchi method background and Implementation

A well-known, user-efficient, inexpensive, and reliable fractional full factorial method called the Taguchi method (TM) allows researchers to study a large number of variables with a limited number of experiments (Ross and Ross 1988; Taguchi et al. 2005). During the design of experiments (DOE), TM centers on the ratio of signal-to-noise (S/N) (where signal refers to the studied response and noise refers to a set of parameters). This S/N ratio uses a specific set of arrays called orthogonal arrays (OA). The S/N ratio acts as a decision variable that helps with data processing and prediction of results trends, whereas the OA generates a certain number of well-balanced experiments. There is an option of selecting the S/N depending on the target of results as smaller, nominal, or larger is better. Since the objective of this study is to maximize the strength, the criteria "larger is better" is considered and the typical equation (1) governed in this case is as follows:

$$\frac{S}{N} = -10log_{10}\left(\frac{1}{n}\sum_{i=1}^{n}\frac{1}{Y_i^2}\right) \qquad (1)$$

Where, "*S/N*" represents the signal-to-noise ratio (in decibels), "*Y"* represents the response, and "*n*" is the number of experiments run in each trial.

In this research, the influence of mixture parameters on the strength of SiMnF, SF, and OPC-based neat, binary blended, and ternary blended binders was assessed using the L9 (i.e., 3^4) array of TM which generated nine trial mixes. Four critical factors with three levels each were studied. The factors were: (A) dosage of SiMnF (%) as a partial replacement of OPC in the range of 0 to 40% at an interval of 20; (B) dosage of SF (%) as a partial replacement of OPC in the range of 0 to 10% at an interval of 5; (C) sand to binder ratio in the range of 1.5 to 2.5 at an interval of 0.5; and (D) water to binder ratio in the range of 0.35 to 0.45 at an interval of 0.5 which are based on common dosage of these materials in cementitious systems. The factors and their levels are summarized in Table 1 while Table 2 presents the L9 orthogonal arrays suggested by TM.

2.2. Material characterizations

Locally available Type I – ordinary Portland cement (OPC) compliant to ASTM C150, silicomanganese fume (SiMnF), and silica fume (SF) were used as the cementitious materials (CMs). The particle size distribution (PSD) of CMs was determined with a laser diffraction technique employing a Malvern Mastersizer 2000. The raw CMs were dispersed in ethanol and kept under an applied ultrasound of 15Hz to avoid particle coagulation. The chemical oxide composition of the CMs was measured using the X-ray fluorescence (XRF) technique in a PANalytic EPSILON 3 XL instrument. The bond characteristics of the CMs (and later, the paste specimens) were identified using a Thermo Fisher's Fourier Transform Infra-red (FT-IR) spectrometer. The physicochemical characteristics of the CMs are detailed in Section 3.1.

Desert sand was used as fine aggregate in all the mortar mixtures. The fineness modulus, water absorption, and bulk-specific gravity of the fine aggregate used were 1.85, 0.65%, and 2.60, respectively. The fineness modulus indicates the sand to be fine sand with reasonable absorption and density. Reticulated tap water was used in the preparation of all mortar and paste mixes.

2.3. Mixture proportions, sample preparation, and testing

The mortar samples were prepared using a Hobart mixer. First, dry mixing of the CMs and the sand was carried out for three minutes for homogeneity followed by the addition of water while the mixing process continued for an additional three minutes. Once the mixing was completed, the flow of each trial mixture was measured as per ASTM C1437 followed by pouring the fresh mortar in 50 mm 3-gang cubic molds and covering the surface with a plastic sheet to limit evaporation. The samples were left undisturbed for approximately 24 hours and cured at ambient conditions in the laboratory (25 ± 3 °C) before being removed from the molds. The strength activity index (SAI) of the mixes was measured at 28 days, as per ASTM C311, whereas the compressive strength of the mortar was evaluated at 3, 7, and 28 days, as per ASTM C109.

Paste specimens (excluding sand) of 25 mm cubic size were also prepared for characterization. It is worth mentioning that in the first stage, the 9 trial mixes suggested by the TM in Table 2 were investigated, while 4 more mixes were developed in the second stage based on the outcome of the first stage. Table 3 summarizes the mixture proportions.

2.4. Morphology

The morphology of the raw CMs, their average diameter, and elemental composition were obtained using the JEOL's JSM-66-10-LV scanning electron microscope (SEM) coupled with the energy dispersive spectroscope (EDS). The paste specimens were also investigated in the SEM to identify changes in the morphological features from the variations in the mixture design parameters. While the raw CMs were spread out on carbon tape for imaging, the paste specimens were embedded in resin. The surface of the investigation was progressively ground on grit papers and polished with liquid diamond for optimum imaging. The surface was then coated with gold and imaging was conducted at 20 kV.

2.5. Bond characteristics

The functional group identification of the raw CMs and the paste specimens was carried out using Thermo Fisher's Fourier Transform Infra-red (FT-IR) spectrometer. The conditions set used during the acquisition of FTIR spectra were: (1) spectral range of 500-4000 cm^{-1} wavenumber, (2) resolution of 4 cm^{-1}, (3) optical speed of 0.63 cm/s, and (4) 32 scans per spectrum.

2.6. Statistical analysis

Based on the response data obtained from optimized mixtures suggested by the Taguchi method, numerical methods were used for various analyses. The statistical significance of each factor on the properties of the developed mortar was determined by the analysis of variance (ANOVA) at a confidence level of 95%. To quantify the effect of the contribution of each factor on the 28-day compressive strength, the sum of squares method was used. The sum of squares was calculated using Equation (2), where N, L, X_i and X' represent the number of specimens tested, the number of levels of the factor, the mean compressive strength for level "*i*" and the mean compressive strength of all experiments, respectively. A multi-linear regression analysis was also carried out to develop a model to predict the compressive strength of the developed mortars.

$$Sum\ of\ squares = N \times L \times \sum_{i=1}^{L} (X' - X_i)^2 \quad (2)$$

2.7. Life cycle assessment (LCA)

In this study, LCA was carried out using the methodology described by ISO (ISO 2006). The LCA framework comprises four phases, including goal and scope, life cycle inventory, impact assessment, and interpretation. The conducted LCA aimed to estimate the environmental impacts of the mixtures and then evaluate their mechanical-environmental efficiency. The global warming potential (GWP) was considered as an environmental index, which evaluates the impact of global warming by equivalent CO_2 emissions. The GWP of the used materials was sourced from the Ecoinvent 3.2 database and available literature (Hong et al. 2012; Iren n.d.; Nazari and Jay G. Sanjayan. 2017; Nematollahi et al. 2017; Ouellet-Plamondon and Habert 2015). Thus, the CO_2 emissions of OPC, SiMnF, SF, sand, and water were taken as 898.0, 4.40, 0.31, 2.30, and 0.11 x 10^{-3} kg·$CO_{2\text{-eq}}$/kg, respectively.

3. Results and discussions

3.1. Characterization of cementitious materials (CMs)

Table 4 summarizes the physicochemical properties of the CMs while Figure 1 displays the particle size distribution (PSD) of SF and SiMnF. The d10, d50, and d90 in Table 4 indicates the particle size below which 10%, 50%, or 90% of all particles are present. The CMs are visually different owing to differences in their composition; the OPC, SF, and SiMnF were grey, dark grey, and dark brown in color, respectively. According to Figure 1, the particle size of SF varied between 16.9 µm (d10) to 235.12 µm (d90) whereas the medium particle size (d50) and the grain span were 85.5 µm and 2.55, respectively. The particle size in SiMnF varied between 0.58 µm (d10) to 180 µm (d90) whereas the medium particle size (d50) and the grain span were 29.17 µm and 6.15, respectively. This shows a significant variation between the grain sizes of SF and SiMnF. The variation of SiMnF particles was more than two folds of that obtained in SF, as evident from the calculated span size. The surface area and pore volume of SiMnF were obtained using a Quantachrome ASiQwin machine. The sample was degassed and analyzed by N2- adsorption-desorption isotherm.

According to the XRF results, the OPC is rich in CaO, SiO_2, and Al_2O_3 (sum = 92.1%), SiMnF is rich in MnO, K_2O, and SiO_2 (sum = 74.2%), whereas SF is rich in SiO_2 and CaO (sum = 89.5%). Even though the sum of SiO_2, Al_2O_3, and Fe_2O_3 was below 50% (minimum standard limit for chemically classifying as Class C type pozzolanic materials), the strength activity index of SiMnF-based (as well as SF-based) test mixture was more than 70% of the control mixture at 28-days (minimum standard limit for physically classifying as Class N, F, or C type pozzolanic materials), as per ASTM C311 (2022), at a 20% cement replacement with the SCMs. This indicates that both CMs possess pozzolanic properties as per ASTM C618 (2022).

3.2. Experimental results

The flow of the trial mortar mixes and the corresponding compressive strengths at 3, 7, and 28 days are presented in Figures 2 and 3, respectively. Mixes with a higher W/C ratio, i.e., a higher water content yielded greater flow. Mixture T1 composed of no SF and made with a water binder ratio of 0.45 exhibited the highest flow. On the other hand, the use of a lower water binder ratio of 0.35 and 0.40 when no SF was used as in T6 and T7, respectively yielded a lower flow compared to that of T1. These results indicate that the incorporation of SF and lower water content would result in a decrease in the flow of the mortars. The decrease in the flow of the mortars when SF was used to replace OPC partially can be linked to the high surface area of the SF as compared to the PC and SiMnF, which consume more water during the reaction, as evident from Table 4. These findings agree with various studies where the use of SF as a partial replacement of OPC has been reported to yield a lower flow (Hamada et al. 2023). Similarly, the decrease in the water available for the cohesion of the components with a lower water-to-binder ratio would result in a decrease in the flow. In contrast to the effect of SF on the flow, it can be noted from T2, T3, and T7 composed of SiMnF as 40% replacement of OPC that incorporation of SiMnF does not result in a high reduction in the flow. This is attributed to the spherical nature of SiMnF particles which imparts a ball-bearing effect in flow mobility as well as due to the dearth of lime in it which is responsible for slow hydration reaction, as observed from the XRF results and strength activity index of SiMnF (Table 4).

It is evident from Figure 3 that the compressive strength of the mortars developed over time as a result of the progressive hydration reaction of OPC and the pozzolanic reaction of SF and SiMnF. The continuous reaction of these binder components over time results in continued product formation and corresponding densification of the microstructure and this is reflected in the increase in compressive strength. It can be noted that mixtures with SiMnF as a partial replacement of OPC exhibited the lowest compressive strength. This could be ascribed to the lower reactivity of SiMnF compared to that of SF and OPC, as also evident from the outcomes of the strength activity index (Table 4).

3.3. Statistical analysis

Analysis of variance (ANOVA) was also carried out and the results are presented in **Table 5**. It can be noted from **Table 5** that the p-values of all the factors are less than 0.05 indicating their statistical significance. The amount of contribution of each factor to the 28-day compressive strength was also investigated by using the sum of squares method. **Figure 4** shows the degree of contribution of each factor. It can be noted from the figure that the content of SiMnF (Factor A) has the highest impact on the compressive strength (76%) followed by water to binder ratio (Factor D) (18%), SF content (Factor B) (4%), and sand-to-binder ratio (Factor C) (2%). The impact of the SiMnF content is also reflected in the 28 days compressive strength; mixes T1, T2, T3, T7, T8, and T9 resulted in a low strength that can be linked to the high content of SiMnF used as a replacement of OPC (i.e., up to 40%) which is rich in MnO, K_2O, and SiO_2 with a low CaO content (Table 4). The water-to-binder ratio is also a critical factor as identified in the ANOVA test confirming the well-known fact that the compressive strength of cementitious materials (mortar in this study) is dependent on the water content utilized in their production (Neville 2010).

Based on the experimental results, a further analysis was also carried out to investigate the influence of the selected factors on the 28-day compressive strength. Figure 5 shows the effect of various factors on compressive strength. It can be noted from Figure 5 that the incorporation of SiMnF, as a partial replacement of the OPC, resulted in a decrease in the compressive strength. This decrease in compressive strength can be linked to the lower reactivity of SiMnF compared to that of OPC, as stated above. SiMnF seems to work as a filler within the timeframe of 28 days as investigated in this study and its pozzolanic reactivity seems to be weaker than that of SF. A recent study (Nasir et al. 2021a) showed that the use of SiMnF as a binder component does not result in any detrimental impact. However, this could be due to the use of the SiMnF in alkali-activated systems, which promotes the dissolution of the monomers in the SiMnF. Thus, to increase the effectiveness of SiMnF in increasing the compressive strength, alkali activators could be incorporated into the mixtures.

On the other hand, the utilization of SF as a partial replacement of OPC resulted in an enhancement in the compressive strength with the use of SF at 5% being the optimum. The improvement in the compressive strength with the replacement of OPC with SF can be ascribed to high strength activity index of 109% of control among all CMs (**Table 4**), which tends to increase its reactivity and consequently increase the binding product formation. Studies have shown that the partial replacement of OPC with low SF content can ensure an improvement in compressive strength (Joshaghani et al. 2018; Roy et al. 2001). These findings also indicate that SF possesses a higher reactivity compared to that of SiMnF.

The increase in the sand-to-binder ratio resulted in a slight reduction in the compressive strength as evident in **Figure 5**. This slight decrease in the compressive strength with the increase in the sand content can be attributed to the reduction in the binder content with the corresponding increase in the sand content. As anticipated, the increase in the water-to-binder ratio resulted in a decrease in compressive strength.

3.4. Optimization and validation

Optimization of the mixtures based on the experimental results was carried out by setting the goal of the optimization process to maximize the compressive strength and include SiMnF and/or SF as partial replacements of the OPC. The best three mixtures from the optimization were selected. To validate the numerical optimization results, four new mixtures comprised of the best three mixtures and the optimum mixture from the trial mixture (i.e., T6) were prepared in the lab to obtain their corresponding experimental results. The factors and their level as well as the composition of the mixtures used for the validation process are presented in **Tables 2** and **3**, respectively.

The results of the predicted compressive strength along with their corresponding experimental values are presented in **Figure 6**. It can be observed that the experimental and predicted compressive strength are comparable within a limit of ± 10%. This is also evident in the good correlation between the experimental and predicted compressive strength as shown in **Figure 7**. Thus, the use of the Taguchi method in the design and analysis of mortar mixtures is an efficient way to optimize mixes with incorporated CMs. The shortlisted mixtures (T6, T11, T12, and T13) which yielded the maximum strength were investigated in detail by analytical techniques in Section 3.5.

3.5. Microstructural Investigation

Figures 8 and 9 depict the SEM micrographs of raw and selected hydrated paste specimens, respectively. It can be observed that SiMnF is partly spherical and smaller than the size of OPC. SF also has a spherical morphology while OPC particles are of irregular polygonal shape. The difference in the morphology can assist identify unreacted particles in the hydrated paste specimens.

Mixture T10, with the maximum compressive strength, has a compact matrix morphology which corroborates its superior strength development pattern identified in Figure 10. In contrast, the morphology of T11 and T12 is not as homogeneous with the presence of pores leading to lower compressive strength in comparison with T10. No pore has been identified in T6 morphology which is also reflected in the compressive strength as compared to T11 and T12. The morphology also confirms that the paste matrix is more homogeneous for T10 with only 5% SF inclusion, confirming the reactive nature of SF in cementitious systems.

The FT-IR spectra of raw CMs and selected paste specimens from Stage 2, validation series in Tables 2 and 3 are shown in Figure 10. The FT-IR spectra of T6 and T10 appear to be similar while that of T11 and T12 are comparable. However, upon close observation, the disparity was evident. For instance, the FT-IR spectra reveal the absence of the bands -OH (3640 cm^{-1} wavenumber) and C-O (1405 and 1475 cm^{-1} wavenumbers), which implies that the composition of portlandite and effects of carbonation, respectively, are lower in T10 in comparison with T6. The occurrence of carbonation is reported to deteriorate the microstructural matrix thereby leading to low-strength development (Pham and Prince 2014; Pizzol et al. 2014). Further, the high strength magnitude in T10 is ascribed to the asymmetric stretching vibration of the Si-O-T chain, as manifested at 950 cm^{-1} wavenumbers, due to the siliceous nature of the SF (SiO_2 = ~93%) as observed by the XRF. This caused more silicate re-organization in the cement matrix and ultimately led to a greater formation of the C-S-H gel and a dense skeletal framework of the T10 specimens.

3.6. Life cycle assessment (LCA)

The CO_2 emissions of all the mixtures are shown in Figure 11. The GWP values ranged from 0.098 to 0.229 kg·CO_2/kg. The highest CO_2 emissions were registered in mixture T6, which contained 100% OPC without any SCMs. On the other hand, the mixes with higher volumes of SiMnF have lower GWP values. For example, mixtures T3 and T7 having 40% SiMnF revealed a CO_2 emissions reduction of around 56.9% and 55.4%, respectively, relative to the reference mixture (T6), as can be seen in Figure 11(b). The carbon footprint breakdown showed that the OPC is the major contributor to the total CO_2 emissions (> 99%), and thus, decreasing its quantity resulted in a significant reduction in the GWP (Figure 11). The contributions of the other ingredients, including SiMnF, SF, and sand, are very minimal (<1%). Thus, the LCA impact of the mixtures is governed by their compositions, mainly the intensive carbon footprint ingredient, e.g., OPC. For further analysis on this point, Figure 11(c) shows the material saving index of all mixtures, where the OPC is taken as the main binder. Interestingly, the data on material saving followed the same trend as the CO_2 emissions reduction. The mixtures T3 and T7 showed a material saving of about 57.4% and 55.9%, respectively.

Since the compressive strength results revealed an adverse effect of the use of high-volume SiMnF, the shortlist mixtures that were optimally selected are discussed further. These mixtures include T6 (OPC), T10 (OPC + SF), T11 (OPC + SiMnF), and T12 (OPC + SF + SiMnF), which reflect different binder systems, i.e., unary, binary, and ternary. The GWP values of T6, T10, T11, and T12 were found to be 0.229, 0.216, 0.182, and 0.170 kg·CO_2/kg, respectively. The mixture with only SF (T10) showed a comparable CO_2 emission to the reference mixture with a reduction of about 5.4%. The higher CO_2 emissions associated with this mixture can be attributed to the low replacement level of OPC by SF (only 5%). The binary and ternary mixtures containing a relatively higher volume of SiMnF (T11 and T12) showed similar CO_2 emissions with a reduction of about 20.3% and 25.6%, respectively. The low CO_2 emissions of T12 are due to the higher replacement level of OPC, where 20% SiMnF plus 5% SF were used in this mixture. The used SiMnF material is an industrial byproduct of the ferroalloy plants, which does not require any post-processing (Nasir et al. 2021b). Consequently, its inclusion in the mixes decreased their overall environmental impact.

To tradeoff between the environmental impact and mechanical performance, an efficiency-based indicator, namely eco-strength efficiency (E_{SE}), was used (Bheel et al. 2022). This indicator accounts for the carbon emissions per unit of functional performance, which here is the compressive strength. It can be noted that the smaller values of E_{SE} indicate good mechanical-environmental efficiency. Figure 12 shows the efficiency indicator of the shortlist mixtures (T6 and T10-12). Comparable results were obtained in all the mixtures. The E_{SE} values at the ages of 7 and 28 days were in the range of 3.41–4.26 and 2.98–3.78x 10^{-3} kg·CO_2·eq/MPa, respectively. The mixture T10 showed the best eco-strength efficiency (an improvement on the benchmarked efficiency to the reference mixture, T6, was about 17.9%). This can be linked to the high compressive strength of T10 among others. Additionally, T12 demonstrated a good efficiency index where its improvement was around 12.5%. Based on the results of the mechanical-environmental efficiency indicator, it can be proposed that the order of the mixtures be as follows: T10 > T12 > T11 > T6. It is also recommended that the expected life of the mixtures be evaluated. Achieving equilibrium expected life by balancing composition factors and LCA is a key concept for sustainable concrete design (Tinoco, de Mendonça et al. 2022, Praticò, Perri et al. 2023).

Conclusions

The effects of OPC substitution by industrial waste and byproducts as SCMs, namely silicomanganese fume (SiMnF) and silica fume (SF), respectively, on the strength, microstructure, and life cycle assessment (LCA) of mortar mixtures were investigated. This was undertaken to trial and test alternative SCMs as the production of fly ash declines globally with power generation shifts its energy source from coal to other alternatives. The Taguchi method for the design of experiments was used to suggest nine different mixtures, representing unary, binary, and ternary systems. Four key factors were investigated – SiMnF (0−40%), SF (0−10%), sand/binder ratio (1.5−2.5), and water/binder ratio (0.35−0.45). The following conclusions could be drawn based on the findings of this study:

- The strength activity index of the mixtures incorporating SMC was more than 70%; however, the mixtures with SiMnF showed a relatively lower reactivity compared to that of OPC.
- The addition of SF decreased the flow of the mortars, while the incorporation of SiMnF had minor effects. In addition, the influence of the water/binder ratio was noticeable in the flow behavior.
- The mixtures with SiMnF, as a partial replacement of OPC, showed the lowest compressive strength among others. In contrast, the utilization of SF, as a partial replacement of OPC, improved the compressive strength, and the results indicated that 5% of SF is the optimum content. This finding can be directly related to the higher pozzolanic reactivity of SF compared to that of SiMnF. The effect of the sand/binder ratio on the compressive strength was found to be insignificant, as shown in the strength reduction trend.
- The ANOVA analysis demonstrated that all the investigated factors had statistical significance on the compressive strength, as evident from the p-values. Moreover, the analysis suggested that the SiMnF incorporation level had the highest impact on the compressive strength, followed by the water/binder ratio, SF content, and sand/binder ratio.
- The optimum mixtures suggested by the Taguchi method were experimentally tested, and a good correlation between the experimental and predicted compressive strengths (R^2 = 0.998) was obtained. This implied the efficiency of the Taguchi method in designing the mortar mixtures and reducing the cost of the experiments.
- Microstructural analysis of the optimally selected mixes revealed that the mixture with an absence of SiMnF showed a compact microstructure with almost no pores, which in turn

resulted in higher compressive strength. This was further supported by the FT-IR spectra, which showed the absence of bands -OH and C-O and the asymmetric stretching vibration of the Si-O-T chain due to the incorporation of SF.

- The mechanical-environmental index of the developed mixtures was assessed using the eco-strength efficiency indicator, which accounts for both the compressive strength and the GWP impact. It was found that the blended mixtures with a relatively high volume of byproducts (~25%) possessed a good efficiency index compared to the OPC-based mixtures; for instance, Mixture T12.

Data Availability Statement

All data, models, and code generated or used during the study appear in this article.

References

American Coal Ash Association (ACAA). 2017. *Production and Use Charts*.

ASTM C311 Standard Test Methods for Sampling and Testing Fly Ash or Natural Pozzolans for Use in Portland-Cement Concrete. 2022.

ASTM C618 Standard Specification for Coal Fly Ash and Raw or Calcined Natural Pozzolan for Use in Concrete. 2022.

Anurag, R. Kumar, S. Goyal, and A. Srivastava. 2021. "A comprehensive study on the influence of supplementary cementitious materials on physico-mechanical, microstructural and durability properties of low carbon cement composites." *Powder Technol*, 394: 645–668. Elsevier B.V. https://doi.org/10.1016/j.powtec.2021.08.081.

Arrigoni, A., D. K. Panesar, M. Duhamel, T. Opher, S. Saxe, I. D. Posen, and H. L. MacLean. 2020. "Life cycle greenhouse gas emissions of concrete containing supplementary cementitious materials: cut-off vs. substitution." *J Clean Prod*, 263: 121465. Elsevier Ltd. https://doi.org/10.1016/j.jclepro.2020.121465.

Bheel, N., M. O. A. Ali, Tafsirojjaman, S. H. Khahro, and M. A. Keerio. 2022. "Experimental study on fresh, mechanical properties and embodied carbon of concrete blended with sugarcane bagasse ash, metakaolin, and millet husk ash as ternary cementitious material." *Environmental Science and Pollution Research*, 29 (4): 5224–5239. Environmental Science and Pollution Research. https://doi.org/10.1007/s11356-021-15954-4.

Gao, T., et al., Analysis of material flow and consumption in cement production process. Journal of Cleaner Production, 2016. 112: p. 553-565.

Gawah, Q., M. A. Al-Osta, M. Maslehuddin, M. A. Abdullah, M. Shameem, and S. U. Al-Dulaijan. 2022. "Development of sustainable self-compacting concrete utilising silico manganese fume." *European Journal of Environmental and Civil Engineering*, 0 (0): 1–22. Taylor & Francis. https://doi.org/10.1080/19648189.2022.2102083.

Hamada, H. M., F. Abed, H. Y. Binti Katman, A. M. Humada, M. S. Al Jawahery, A. Majdi, S. T. Yousif, and B. S. Thomas. 2023. "Effect of silica fume on the properties of sustainable cement concrete." *Journal of Materials Research and Technology*, 24: 8887–8908. https://doi.org/https://doi.org/10.1016/j.jmrt.2023.05.147.

Hong, T., C. Ji, and H. Park. 2012. "Integrated model for assessing the cost and CO 2 emission (IMACC) for sustainable structural design in ready-mix concrete." *J Environ Manage*, 103: 1–8. Elsevier Ltd. https://doi.org/10.1016/j.jenvman.2012.02.034.

Iren, T. n.d. "Environmental Aspects of Utilising Silicomanganese Slag as a Cement Substitute." University of Agder Norway.

ISO. 2006. *Environmental Management - Life Cycle Assessment, Principles and Framework: 14040*. Geneva: International Organization for Standardization.

Joshaghani, A., M. A. Moeini, M. Balapour, and A. Moazenian. 2018. "Effects of supplementary cementitious materials on mechanical and durability properties of high-performance non-shrinking grout (HPNSG)." *J Sustain Cem Based Mater*. https://doi.org/10.1080/21650373.2017.1372318.

Nasir, M., M. A. M. Johari, A. Adesina, M. Maslehuddin, M. O. Yusuf, M. J. A. Mijarsh, M. Ibrahim, and S. K. Najamuddin. 2021a. "Evolution of room-cured alkali-activated silicomanganese fume-based green mortar designed using Taguchi method." *Constr Build Mater*. https://doi.org/10.1016/j.conbuildmat.2021.124970.

Nasir, M., M. A. M. Johari, A. Adesina, M. Maslehuddin, M. O. Yusuf, M. J. A. Mijarsh, M. Ibrahim, and S. K. Najamuddin. 2021b. "Evolution of room-cured alkali-activated silicomanganese fume-based green mortar designed using Taguchi method." *Constr Build Mater*, 307 (September): 124970. Elsevier Ltd. https://doi.org/10.1016/j.conbuildmat.2021.124970.

Nasir, M., M. A. Megat Johari, M. Maslehuddin, and M. Olalekan Yusuf. 2020. "Magnesium sulfate resistance of alkali/slag activated silico-manganese fume-based composites." *Constr Build Mater*, 265: 120851. https://doi.org/10.1016/j.conbuildmat.2020.120851.

Nasir, M., M. A. Megat Johari, M. Maslehuddin, and M. O. Yusuf. 2021c. "Sulfuric acid resistance of alkali/slag activated silico-manganese fume-based mortars." *Structural Concrete*, 22 (S1). https://doi.org/10.1002/suco.201900543.

Nazari, A., and Jay G. Sanjayan. 2017. *Handbook of Low Carbon Concrete*. (Butterworth-Heinemann, ed.). Kidlington, UK.

Nematollahi, B., J. Sanjayan, J. Qiu, and E. H. Yang. 2017. "Micromechanics-based investigation of a sustainable ambient temperature cured one-part strain hardening geopolymer composite." *Constr Build Mater*, 131: 552–563. Elsevier Ltd. https://doi.org/10.1016/j.conbuildmat.2016.11.117.

Neville, A. M. 2010. *Properties of Concrete*. London, UK: Pearson Education Limited.

Ouellet-Plamondon, C., and G. Habert. 2015. *Life cycle assessment (LCA) of alkali-activated cements and concretes*. *Handbook of Alkali-Activated Cements, Mortars and Concretes*. Woodhead Publishing Limited.

Pham, S. T., and W. Prince. 2014. "Effects of carbonation on the microstructure of cement materials: influence of measuring methods and of types of cement." *Int J Concr Struct Mater*, 8: 327–333. Springer.

Pizzol, V. D., L. M. Mendes, L. Frezzatti, H. Savastano Jr., and G. H. D. Tonoli. 2014. "Effect of accelerated carbonation on the microstructure and physical properties of hybrid fiber-cement composites." *Miner Eng*, 59: 101–106. https://doi.org/https://doi.org/10.1016/j.mineng.2013.11.007.

Praticò, F.G., et al., Comparing bio-binders, rubberised asphalts, and traditional pavement technologies. Construction and Building Materials, 2023. 400: p. 132813.

Ross, P. J., and P. J. Ross. 1988. *Taguchi techniques for quality engineering: loss function, orthogonal experiments, parameter and tolerance design*. McGraw-Hill New York.

Roy, D. M., P. Arjunan, and M. R. Silsbee. 2001. "Effect of silica fume, metakaolin, and low-calcium fly ash on chemical resistance of concrete." *Cem Concr Res*, 31 (12): 1809–1813. https://doi.org/10.1016/S0008-8846(01)00548-8.

Santos, T., J. Almeida, J. D. Silvestre, and P. Faria. 2021. "Life cycle assessment of mortars: A review on technical potential and drawbacks." *Constr Build Mater*, 288: 123069. Elsevier Ltd. https://doi.org/10.1016/j.conbuildmat.2021.123069.

Taguchi, G., S. Chowdhury, and Y. Wu. 2005. Taguchi's quality engineering handbook. Wiley.

Tinoco, M.P., et al., Life cycle assessment (LCA) and environmental sustainability of cementitious materials for 3D concrete printing: A systematic literature review. Journal of Building Engineering, 2022. 52: p. 104456.

Table 1. Factors and levels used in experimental design.

Factor		Level		
		1	2	3
A	SiMnF (%)	0	20	40
B	SF (%)	0	5	10
C	Sand/Binder ratio	1.5	2	2.5
D	Water/Binder ratio	0.35	0.4	0.45

Table 2. Taguchi method of the orthogonal array.

Stages	Trial Run	Factor A	Factor B	Factor C	Factor D
		SiMnF (%)	SF (%)	Sand/Binder mass ratio	Water/Binder mass ratio
Stage 1 (Trial mixes)	T1	20	0	2	0.45
	T2	40	5	1.5	0.45
	T3	40	10	2	0.35
	T4	0	10	2.5	0.45
	T5	0	5	2	0.40
	T6	0	0	1.5	0.35
	T7	40	0	2.5	0.40
	T8	20	5	2.5	0.35
	T9	20	10	1.5	0.40
Stage 2 (Validation)	T6	Repeat as above			
	T10	0	5	1.5	0.35
	T11	20	0	1.5	0.35
	T12	20	5	1.5	0.35

Table 3. Composition of mixtures for trial and validation (kg/m³).

Stages	Trial Run	OPC	SiMnF	SF	Sand	Water
Stage 1 (Trial mixes)	T1	514.5	128.6	0	1286.2	289.4
	T2	401.1	291.7	36.4	1094.0	328.2
	T3	339.7	271.8	67.9	1359.1	237.8
	T4	512.9	0	56.9	1424.9	256.4
	T5	631.6	0	33.2	1329.8	265.9
	T6	797.8	0	0	1196.7	279.2
	T7	351.6	234.4	0	1465.0	234.4
	T8	453.0	120.8	30.2	1510.1	211.4
	T9	530.2	151.5	75.7	1136.3	303.0
Stage 2 (Validation)	T6	Repeat as above				
	T10	754.8	0	39.7	1191.7	278.0
	T11	635.1	158.7	0	1190.8	277.8
	T12	592.9	158.1	39.5	1185.9	276.7

Table 4. Physical and chemical characteristics of the cementitious materials.

	Physical properties			Chemical composition			
Characteristics	OPC	SF	SiMnF	Oxide Wt. (%)	OPC	SF	SiMnF
Color	Grey	Dark Grey	Dark Brown	CaO	64.50	5.76	7.25
Particle shape	Irregular	Spherical to polygonal	Spherical	MnO	-	0.11	35.40
Specific gravity	3.15	2.37	2.87	SiO_2	21.90	83.76	19.50
Surface area (m^2/g)	-	-	10.06	K_2O	0.35	2.27	16.60
Pore volume (cm^3/g)	-	-	0.0001	Al_2O_3	5.70	2.10	1.45
Grain size (µm), d_{10}	0.79	16.9	0.58	SO_3	-	1.95	6.25
Grain size (µm), d_{50}	9.30	85.5	29.17	MgO	2.10	0.95	5.70
Grain size (µm), d_{90}	20.10	235.12	179.95	Fe_2O_3	3.70	2.23	3.35
Grain span $(d_{90}-d_{10})/d_{50}$	2.07	2.55	6.15	Loss on Ignition (LOI)	0.65	0.85	5.82
28-d SAI (%)	-	109	76				

Table 5. ANOVA on 28 days compressive strength.

Factors	Degree of freedom	Sum of squares	Variance	p-value	Contribution on strength
A	2	1142.3	571.13	0.0007	76%
B	2	56.19	28.10	0.0046	4%
C	2	35.76	17.88	0.0039	2%
D	2	273.54	136.77	0.0032	18%
Total	8				100%

Figure Captions

Figure 1. Particle size distribution of raw SF and SiMnF.

Figure 2. The flow of mortars.

Figure 3. Compressive strength of mortars.

Figure 4. Contribution of factors on compressive strength.

Figure 5. Effect of factors on compressive strength.

Figure 6. Experimental and predicted compressive strength of mixtures used for validation.

Figure 7. Correlation between experimental and predicted results.

Figure 8. SEM micrographs of the raw cementitious materials.

Figure 9. SEM micrographs of the paste specimens.

Figure 10. FT-IR spectra of the raw and paste specimens.

Figure 11. LCA analysis: (a) CO_2 emissions; (b) Reduction in emissions; and (c) Material savings.

Figure 12. Eco-strength efficiency of the shortlist mixtures.

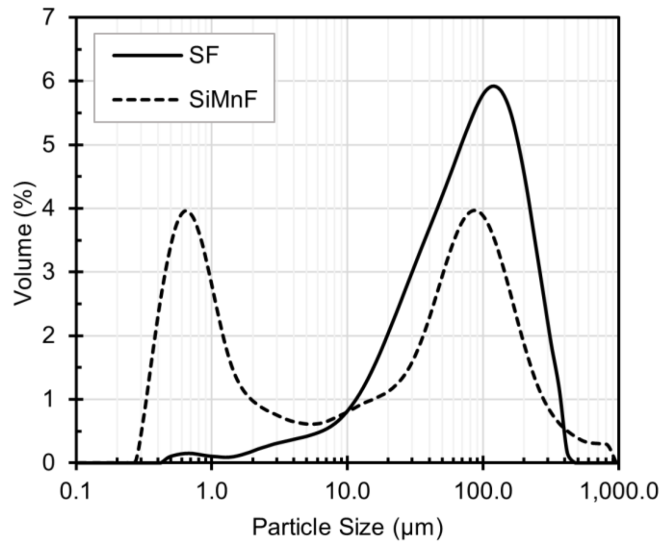

Figure 1. Particle size distribution of raw SF and SiMnF.

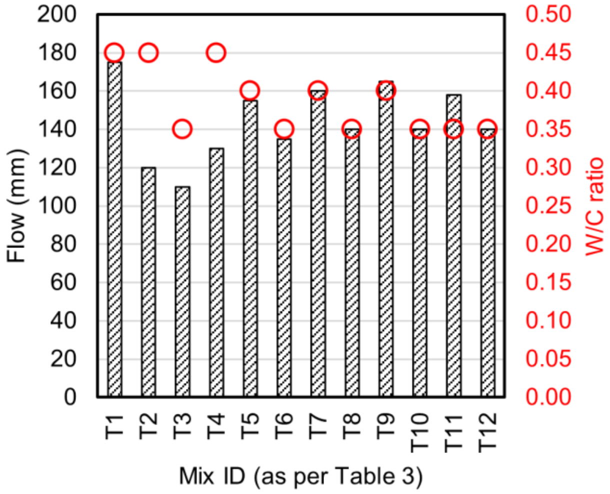

Figure 2. The flow of mortars.

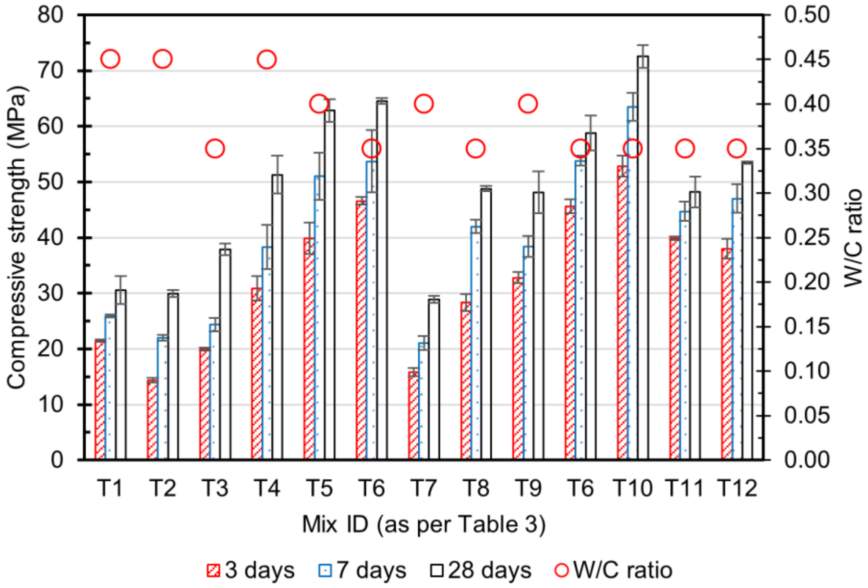

Figure 3. Compressive strength of mortars.

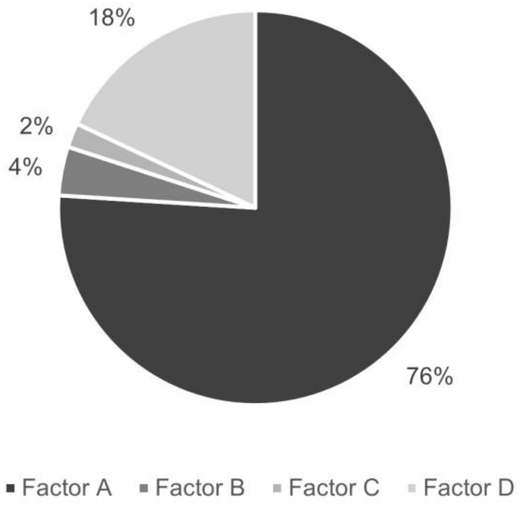

Figure 4. Contribution of factors on compressive strength.

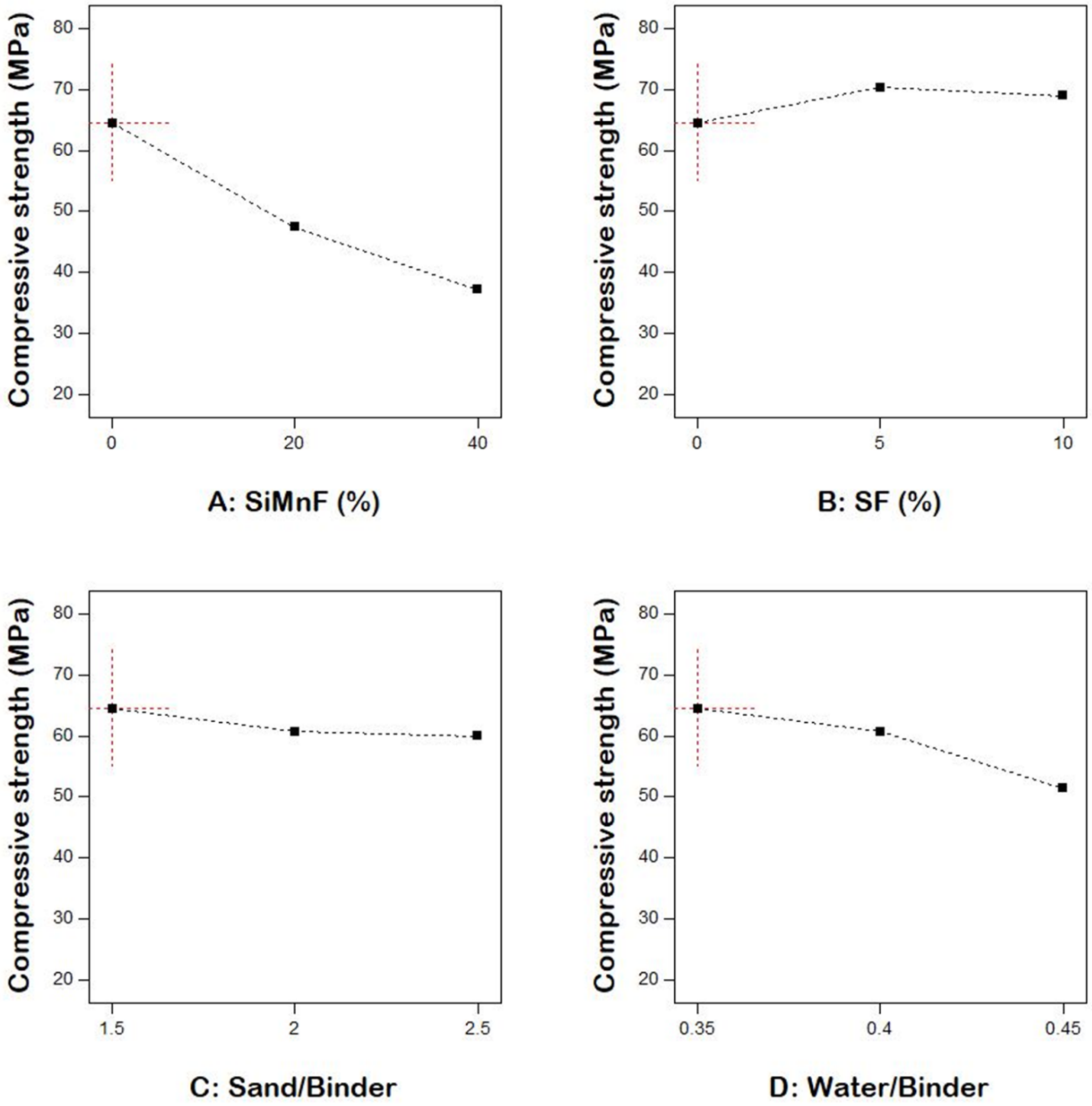

Figure 5. Effect of factors on compressive strength.

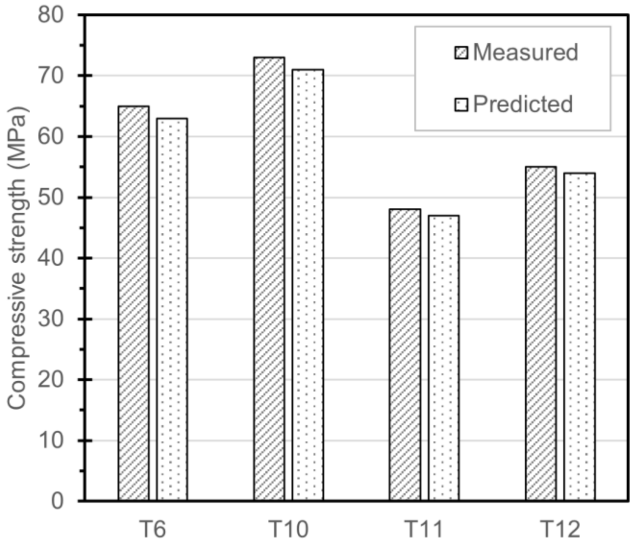

Figure 6. Experimental and predicted compressive strength of mixtures used for validation.

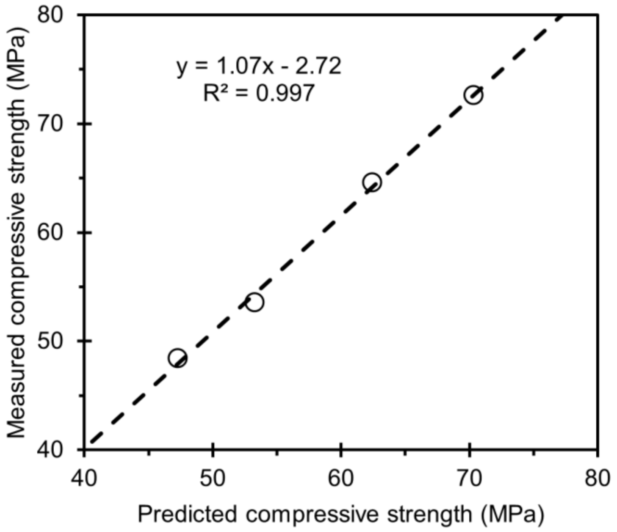

Figure 7. Correlation between experimental and predicted results.

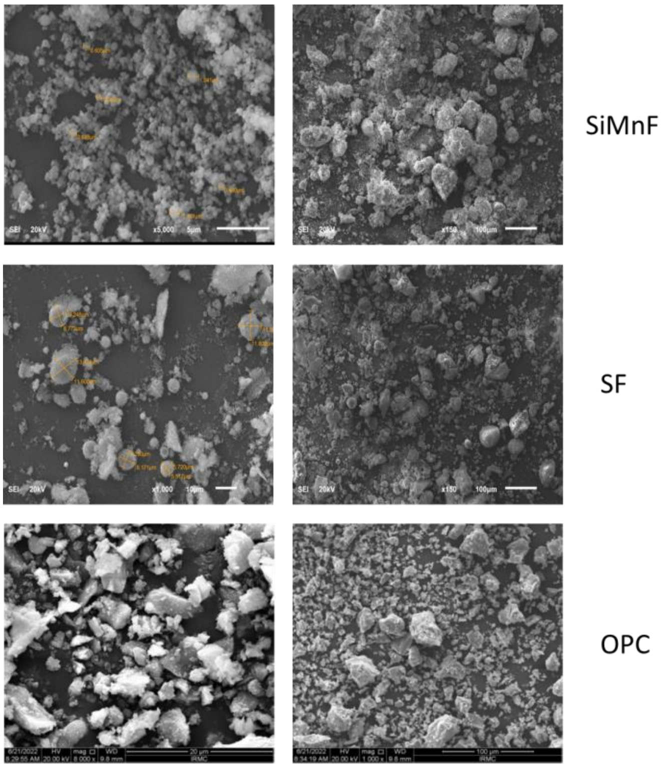

Figure 8. SEM micrographs of the raw cementitious materials.

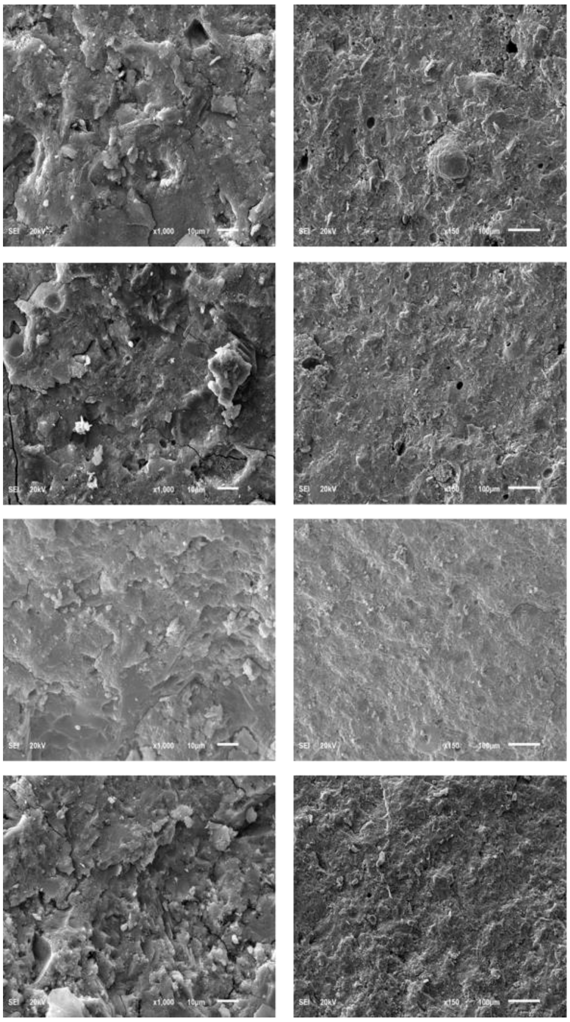

Figure 9. SEM micrographs of the paste specimens.

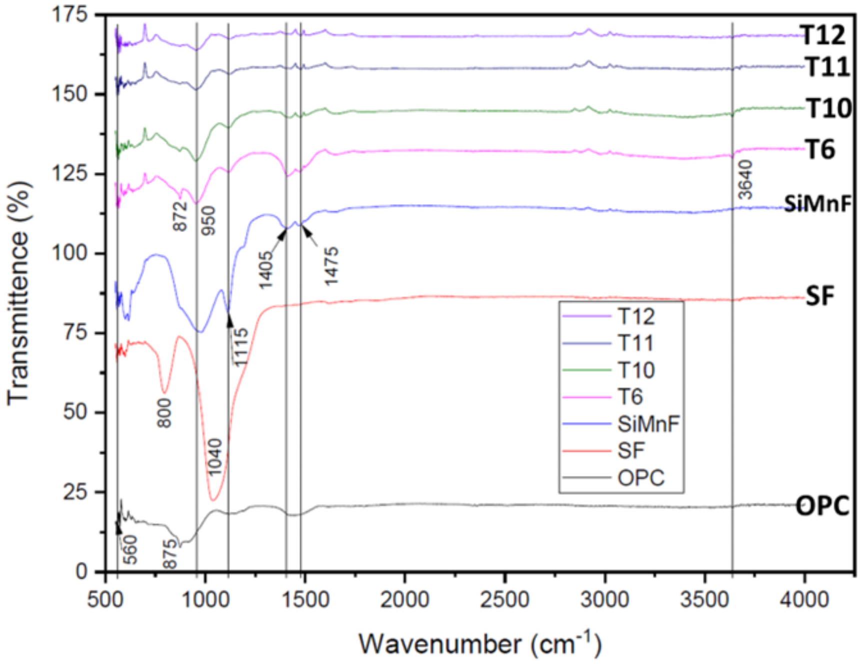

Figure 10. FT-IR spectra of the raw and paste specimens.

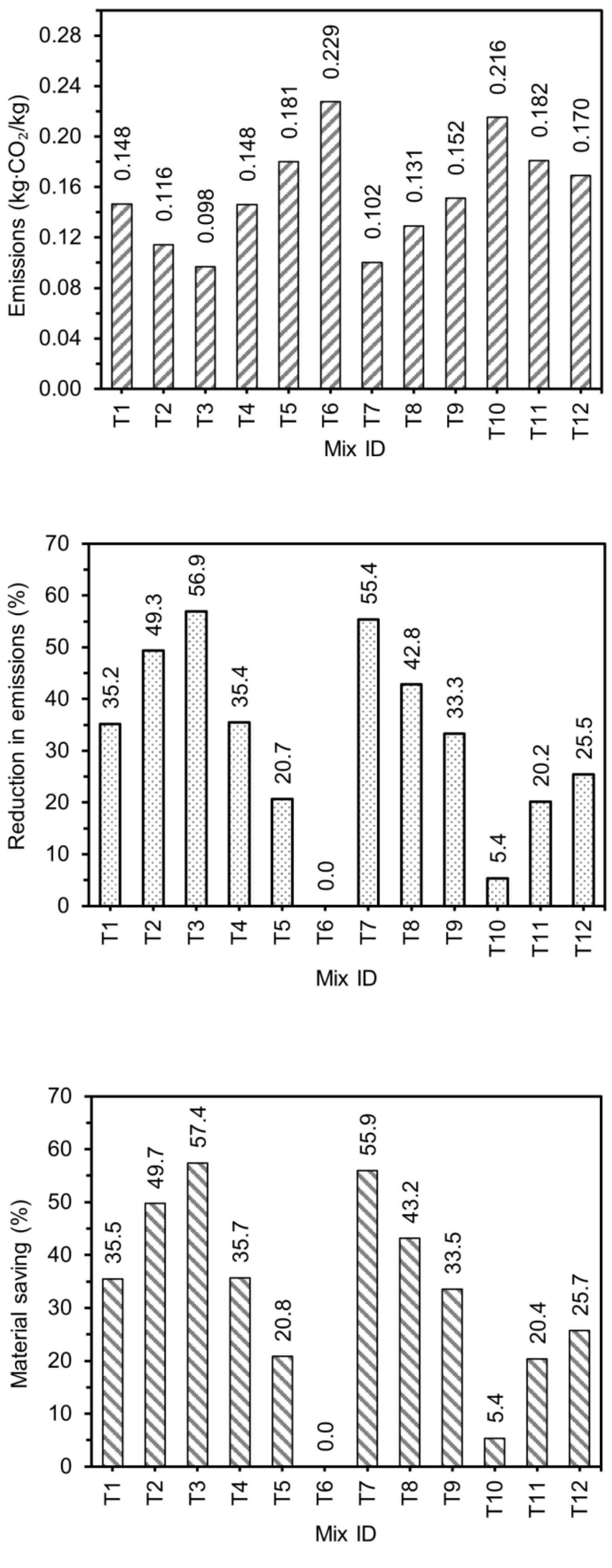

Figure 11. LCA analysis: (a) CO_2 emissions; (b) Reduction in emissions; and (c) Material savings.

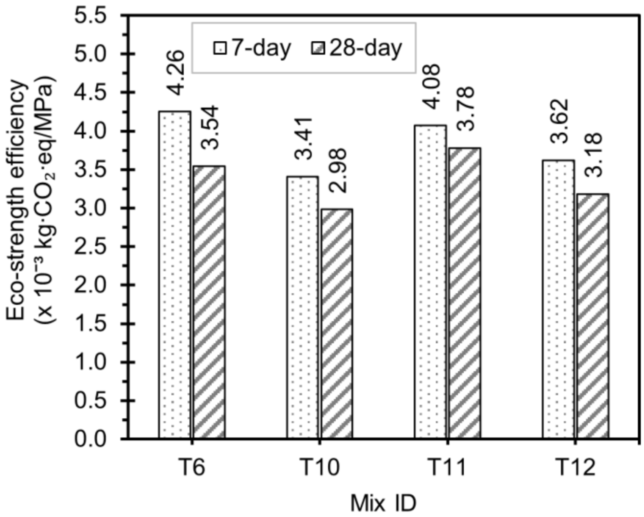

Figure 12. Eco-strength efficiency of the shortlist mixtures.